Competition is a driving force in topographic mapping

Jason W. Triplett[a,1], Cory Pfeiffenberger[a,1], Jena Yamada[a], Ben K. Stafford[a], Neal T. Sweeney[a], Alan M. Litke[b], Alexander Sher[b,c], Alexei A. Koulakov[d,2], and David A. Feldheim[a,2]

[a]Department of Molecular, Cell, and Developmental Biology, [b]Santa Cruz Institute of Particle Physics, and [c]Department of Physics, University of California, Santa Cruz, CA 95064; and [d]Cold Spring Harbor Laboratory, Cold Spring Harbor, NY 11724

Topographic maps are the primary means of relaying spatial information in the brain. Understanding the mechanisms by which they form has been a goal of experimental and theoretical neuroscientists for decades. The projection of the retina to the superior colliculus (SC)/tectum has been an important model used to show that graded molecular cues and patterned retinal activity are required for topographic map formation. Additionally, interaxon competition has been suggested to play a role in topographic map formation; however, this view has been recently challenged. Here we present experimental and computational evidence demonstrating that interaxon competition for target space is necessary to establish topography. To test this hypothesis experimentally, we determined the nature of the retinocollicular projection in Math5 (Atoh7) mutant mice, which have severely reduced numbers of retinal ganglion cell inputs into the SC. We find that in these mice, retinal axons project to the anteromedial portion of the SC where repulsion from ephrin-A ligands is minimized and where their attraction to the midline is maximized. This observation is consistent with the chemoaffinity model that relies on axon–axon competition as a mapping mechanism. We conclude that chemical labels plus neural activity cannot alone specify the retinocollicular projection; instead axon–axon competition is necessary to create a map. Finally, we present a mathematical model for topographic mapping that incorporates molecular labels, neural activity, and axon competition.

Most sensory information is mapped topographically, meaning that the neighbor relationships among neurons are maintained when choosing synaptic partners in their target area. The visual projection from the retina to the superior colliculus (SC) has been widely used as a model to ascertain the mechanisms by which topographic maps develop. In the retinocollicular projection, the dorsal–ventral (D–V) axis of the retina maps topographically onto the medial–lateral (M–L) axis of the SC, and the temporal–nasal (T–N) axis maps onto the anterior–posterior (A–P) axis of the SC (1, 2). These two axes are mapped by independent mechanisms (3).

Topographic mapping along each axis is believed to rely upon counterbalanced forces (4, 5). Dual molecular gradient models propose that separate repellent or attractant molecules coexist in opposing gradients and that the balance point of the two gradients determines the appropriate termination locus for retinal axons (hereafter called the dual gradient model) (4, 6–8). Servomechanism models posit that a single graded molecule can have both positive and negative effects that serve to guide retinal axons to their correct position (9–13). Still other models invoke a counterbalancing force that is generated via axonal competition for space or positive factors in the target (5, 14–19). Although all of these models include competition as a factor to ensure that axons spread to fill the available target space, only competition models invoke competition as a nonredundant mapping mechanism that is necessary for axons to terminate at correct locations. Testing the role of competition can help understand the chemoaffinity mechanism involved in the topographic map formation.

A number of experiments have tested the role of competition in topographic mapping with differing conclusions as to its role. Ablation studies performed in amphibians, fish, and rodents have

shown that retinal ganglion cell (RGC) axons can fill the available target space after partial ablation of the retina or tectum/SC while maintaining topographic order. This result is taken to demonstrate that axons normally compete for target space and sort out on the basis of their relative rather than absolute sensitivities to guidance molecules. However, ablation experiments do not distinguish between the three mapping mechanisms described above, because each of them includes competition as a means to fill available target space. Regenerating axons in fish and frogs create more ordered maps after ablation than those of rodents, suggesting that there may be differences in the degree of competition used between cold- and warm-blooded species (9, 20–22). In addition, the findings that topographic maps rearrange after disruption of EphA and ephrin-A gradients in mice suggest that there is not a strict gradient-matching mechanism for topography (14, 15, 23). On the other hand, Gosse et al. have challenged a requirement for competition in topographic mapping (24). Instead of lesions to reduce competition, a single RGC was transplanted into a mutant zebrafish that lacked RGCs. They found that the distal tips of solitary axons projected to the topographically correct position but had more arbors anterior to the correct position than under crowded conditions, suggesting that topographic order can be established without competition (most consistent with the dual gradient and servomechanism models), but that competition is involved in pruning RGC arbors during topographic map refinement (24).

Here, we simulate different mapping models using a common mathematical framework to define several possible outcomes when axonal competition is drastically reduced. To test which of these models best describes what occurs in mammals, we traced projections from the retina to the SC in Math5 (Atoh7) mutant mice (25, 26). Math5 mutants have 5–10% of the normal amounts of RGCs that are spread evenly across the retina (27). These RGCs will therefore experience less competition for target-derived factors in the SC than they do in wild type (WT) mice, providing a non-lesion paradigm to study the role of competition in mammals. We find that in contrast to WT mice, in which RGCs fill the entire SC, RGC axons in Math5 mutants are enriched in the anteromedial SC. This result is most consistent with models that include axon competition as a counterbalancing force in topographic mapping.

Results

Different Mapping Models Predict Different Outcomes When RGC Numbers Are Reduced. To provide quantitative predictions for the structures of topographic maps resulting from a decrease in RGC

axon numbers, we reformulated the competition, dual-gradient, and servomechanism models into a common mathematical framework. The assumptions underlying each of these models are detailed below and in the *SI Appendix*. First, we considered mapping from the T–N axis of the retina onto the A–P axis of the SC (Fig. 1). Each model incorporates experimental evidence demonstrating that a posterior-to-anterior SC gradient of ephrin-A repellent activity is differentially detected by RGC axons. EphA receptors are expressed by RGCs in a low-nasal to high-temporal gradient, which results in temporal axons being more sensitive to ephrin-As than nasal axons, causing them to terminate in the anterior SC (15). These models differ in the explanation of why nasal axons that contain very low levels of EphA terminate in the posterior SC. The competition model postulates that competitive interactions with temporal axons force axons to terminate further up a repulsive ephrin-A gradient (Fig. 1*A*). In the servomechanism model, the interaction with ephrin-As is more complex than simple repulsion. Thus, responses to ephrin-As may change, depending on the origin of an RGC along the T–N axis, such that the same axon may be repelled by high levels of ephrin-A but attracted by lower levels (10, 28, 29). As a result, there is a specific point for each axon where the interaction changes from repulsion to attraction (dashed line in Fig. 1*B*). This balance point determines the position of axonal termination zones and depends on EphA levels on the axon, thus creating an ordered topographic map (10). Finally, the dual gradient model suggests that the counterbalancing force is provided by a different label that, for example, is expressed in a gradient counter to ephrin-As (Fig. 1*C*). Candidates for this second label are EphAs expressed in the SC in an anterior-to-posterior gradient. EphAs may interact with ephrin-As that are expressed more highly in nasal RGCs, thus initiating reverse signaling through these GPI-linked proteins (30–32). Such an interaction would result in nasal RGCs being repelled to the posterior SC.

Similar versions of these models also exist for sorting axons along the M–L axis of the SC according to their D–V origin in the retina. Mapping along this axis is thought to be dependent on EphB/ephrin-B interactions; the former has a low-dorsal to high-ventral retinal distribution, whereas the latter displays a low-lateral to high-medial collicular gradient (33). Because ventral RGCs, with high EphB expression, map to the medial SC, where ephrin-B expression is highest, the interactions between these labels are predicted to be attractive (34). With this modification, the same three mapping models could be used to explain how the D–V to M–L projection is formed. Because each axis is mapped independently, different mechanisms could be used on each, resulting in nine possible pairs of models to explain how topography is established in the SC. Indeed, use of any combination of models predicts the formation of an orderly topographic map when normal numbers of RGCs are included (*SI Appendix*, Fig. S1).

To theoretically test the role of competition in topographic mapping, we ran simulations of mapping for reduced numbers of RGC inputs resulting in nine different predictions about where RGC axons will terminate (Fig. 2). For example, if the competition model is implemented along the T–N (azimuth) axis, axons project to regions where the density of ephrin-As is minimal, in anterior SC. This is because ephrin-As act solely as repellents in this model and nasal axons that project to the posterior SC in WT mice merge with temporal axons because the counterbalancing force of competition is reduced (Fig. 2 *B*, *E*, and *H*). Similarly, when the competition model is implemented along the D–V axis, RGC axons group medially at locations of maximal ephrin-B, which is an attractant (Fig. 2 *B–D*). Along the T–N axis, the dual gradient model leaves topographic order intact under reduced competition. This is because each axon detects repulsive labels coming from each end of the A–P axis and can find its topographically correct location even in the absence of competition from other axons. If a dual gradient model is used along the D–V axis, a split map is formed (Fig. 2 *H–J*). This is because in a dual gradient model with attractive labels, equilibrium points for each axon are unstable, making all axons project

Fig. 1. Three models to explain how topography is formed along the T–N axis of the visual world using counterbalancing forces. Each model incorporates the posterior-to-anterior collicular gradient of ephrin-A repellent activity detected by a temporal-to-nasal gradient of EphA in the retina (shaded triangles) as one force (downward arrow in all panels). The models differ in the origins of the counterbalancing force (upward arrow) that determines the axon termination loci (triangles). (*A*) In competition models the counterbalancing force is in the competitive interactions with temporal axons that pushes all other axons up the repulsive gradient. (*B*) In servomechanism models, the same axon is both attracted and repelled by ephrin-As. As a result, an axon terminates at a point of balance between repulsion and attraction (dashed line). (*C*) Dual gradient models suggest that the repulsion of ephrin-As is counterbalanced by another repellent label that is expressed in a counter gradient, such as EphAs. In these models, collicular EphA interacts with ephrin-A expressed by retinal axons. A, anterior; P, posterior; L, lateral; M, medial.

Fig. 2. Models for topographic mapping make different predictions of the structure of retinal maps in the SC when the number of axons is reduced to 5%. (*A*) Topographic map for a complete set of axons. The average position of axon origin in retina is color coded using the color map given in the retinal map. The gradients of chemical labels are shown schematically. This map is obtained when the competition model is implemented along both axes. For the complete set of axons, all nine mapping mechanisms yield similar results (*SI Appendix*, Fig. S1). (*B–J*) Maps for nine combinations of mapping mechanisms along two perpendicular retinal axes (T–N and D–V) when 5% of retinal axons chosen randomly are included in the model as in the Math5−/− mice. The dark oval region represents the collicular locations available for axons. The number of synapses at each collicular locus is represented by the brightness of the map. Synapses of retinal axons occupy a subset of collicular loci, which is dependent on the combination of mapping mechanisms.

NEUROSCIENCE

to the edges of the map where the densities of two attractants (ephrin-Bs and EphBs) are maximal. In contrast, modeling of the servomechanism along the M–L axis predicts a normal map under conditions of reduced competition (Fig. 2 *E–G*). In conclusion, the three chemoaffinity mechanisms (Fig. 1) make strikingly different predictions as to whether RGC axons fill the entire SC or whether large areas of the SC will remain devoid of inputs in situations where competition is reduced. Therefore, analysis of the retinocollicular projection under conditions of reduced competition will allow the determination of the counterbalancing force that regulates retinocollicular map formation and can distinguish between various chemoaffinity mechanisms (Fig. 2).

RGC Axons in Math5 Mutants Are Restricted to the Anteromedial SC.
To determine which model best corresponds to the actual mechanism of topographic mapping, we traced the whole eye's projection to the SC in adult and early postnatal stages for WT, heterozygous Math5 (Math5$^{+/-}$), and homozygous Math5 (Math5$^{-/-}$) mutant mice (Math5$^{+/-}$ mice have normal numbers of RGCs, and exhibit WT expression levels and cell numbers) (35). Injection of fluorescently tagged cholera toxin B (CTB) into the eye of both WT and Math5$^{+/-}$ adult mice shows that RGC axons fill the entire contralateral SC evenly along each axis (Fig. 3 *A* and *B*). Similar injections tracing the RGC axons of Math5$^{-/-}$ mice show that they do not fill the entire SC, but rather are enriched in the anteromedial part, leaving large areas of the SC without substantial terminations (Fig. 3*C*). The anterior/medial enrichment of RGCs can be detected as early as postnatal day 2 (P2), an age before the completion of RGC refinement in the mouse (22) (Fig. 3 *F* and *G*). These data agree well with predictions of the competition model along both axes in Fig. 2*B* and therefore support competition as a counterbalancing force, which is necessary for correct topographic map formation along both A–P and D–V retinal axes. One small inconsistency from what we observe and the competition model is a decrease in fluorescence at the extreme anterior edge of the SC. This is the area of highest EphA expression, which has been shown to repel both temporal and nasal axons in vitro (32). Nonetheless, a detailed quantitative comparison between computational and experimental results for all models shows that the competition model best fits our observed experimental data (*SI Appendix*, Fig. S2).

Anatomical Tracing of the Retinocollicular Projection in Math5$^{-/-}$ Mice.
Whereas whole eye tracings show that the retinocollicular projection is compressed in Math5$^{-/-}$ mice, they cannot determine whether there is any structure within the compressed projection. To assay structure this, we retrogradely traced retinocollicular projections in WT, Math5$^{-/-}$, and Math5$^{+/-}$ mice by focal injection of red and green CTBs into the SC at P8–P10 and examined the contralateral retina 2 d later. We find that in WT and Math5$^{+/-}$ mice, a single injection into the SC retrogradely labels a cluster of RGCs that originate in the topographically correct part of the retina (Fig. 4 *A–C*). Similar injections within the anterior–medial SC of Math5$^{-/-}$ mice retrogradely label RGCs that are dispersed throughout the retina (Fig. 4 *E–G*). We quantified the number of retrogradely labeled RGCs across the N–T axis of the retina. In Math5$^{+/-}$ animals, clusters of labeled RGCs were found in the topographically appropriate location. In contrast, similarly placed injections in Math5$^{-/-}$ mice show a broad distribution of RGCs across the retina, with the anterior SC injections showing a slightly more temporal distribution than more posterior injections (Fig. 4 *D* and *H*). In addition, retrograde tracing from lateral SC failed to label RGCs in the retina, confirming that this part of the SC is not innervated by the retina (*SI Appendix*, Fig. S3). Attempts to anterogradely trace RGCs of Math5 mutants were difficult because of the reduced number of RGCs in the retina. However, in a few cases, we were able to label RGCs anterogradely in Math5$^{-/-}$ mutants by focal 1,1'-
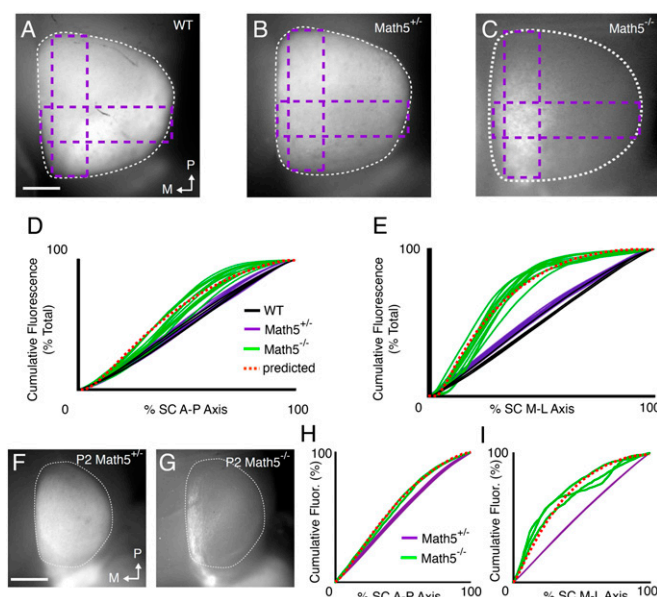
Fig. 3. RGCs project to the medioanterior SC in Math5$^{-/-}$ mice. (*A–C*) Whole mount fluorescence images of the SC from adult WT (*A*), Math5$^{+/-}$ (*B*), and Math5$^{-/-}$ (*C*) mice and P2 Math5$^{+/-}$ (*F*) and Math5$^{-/-}$ (*G*) mice, after injection of fluorescent anterograde tracer in the contralateral eye. White dotted lines show the dimensions of the SC; posterior is at the *Top*, medial to the *Left*. Purple dotted lines show the regions quantified in *D* and *E*. M, medial; P, posterior. (*D*, *E*, *H*, and *I*) Fluorescent intensity profiles of injected mice. The graphs plot the percent of total intensity as a function of A–P (*D* and *H*) or M–L (*E* and *I*) position. Whereas WT and Math5$^{+/-}$ mice have an approximate linear intensity profile, the profiles of Math5$^{-/-}$ mice plateau before reaching the posterior and lateral borders. Black lines are individual WT mice, purple lines are individual Math5$^{+/-}$ mice, and green lines are individual Math5$^{-/-}$ mice. Dashed red lines are the results of the computational model shown in Fig. 2*B* (competition model along both axes). Modeling results in *H* and *I* reflect incomplete simulations (15% of the number of steps used in Fig. 2*B*). Adults: WT, $n = 4$; Math5$^{+/-}$, $n = 7$; Math5$^{-/-}$, $n = 8$. P2: Math5$^{+/-}$, $n = 3$; Math5$^{-/-}$, $n = 2$. (Scale bar, 250 μm.)

dioctadecyl-3,3,3',3'-tetramethylindocarbocyanine (DiI) injection into the retina. In these cases we find that nasal RGCs do not form obvious termination zones, are spread along the A–P axis of the SC, and temporal RGCs have arbors that remain in the anterior portion of the SC (Fig. 4 *I–L*). Taken together, these results suggest that there is some topographic order of RGCs within the compressed region of the Math5$^{-/-}$ retinocollicular projection.

These data are consistent with our modeling, which shows reduced topographic order when the number of RGCs is reduced (Fig. 2). Retrograde tracings in Math5$^{-/-}$ mice lead to a scatter of RGCs in the retina with the SD of 22% (Fig. 4*H*). Modeling data show similar SD of about 20% along the T–N or D–V axis (*SI Appendix*, Fig. S9 *C* and *D*). The map precision is reduced in retrograde labeling compared with the WT case (~5%, *SI Appendix*, Fig. S9 *A* and *B*), because of slower refinement in Math5$^{-/-}$ conditions due to the reduced density of synapses (*SI Appendix*, Fig. S12).

Individual RGCs in Math5 Mutant Mice Are Functional.
Whereas it has been shown that the RGCs that remain in the Math5$^{-/-}$ retina are evenly distributed throughout the N–T and D–V axes of the retina (27), it is possible that the compressed retinal projection in the SC in Math5$^{-/-}$ mice is due to altered retinal development that leads to changes in the expression patterns of axon guidance molecules and/or activity profiles of individual RGC neurons, which could cause them to make targeting errors.

Fig. 4. Anatomical tracing of the retinocolliculuar projection in Math5$^{-/-}$ mice. (*A–C*) Injection of CTB-488 (green) and CTB-555 (red) in adjacent anterior–posterior SC locations retrogradely labels adjacent clusters of RGCs in the temporal retina of Math5 heterozygous mice (arrows) with few labeled RGCs distal from the cluster. (*D*) Quantification of the fluorescence in equal-sized bins across the temporal–nasal axis reveals sharp peaks in adjacent bins in temporal retina in Math5$^{+/-}$ mice (*n* = 3). (*E–G*) Similar injections in Math5$^{-/-}$ mice retrogradely label RGCs that originate from widespread areas of the retina. (*H*) Quantification of the fluorescence found in equal-sized bins across the temporal–nasal axis reveals a broad distribution of label, with a slight bias toward the temporal and nasal retina for anterior and posterior injection sites, respectively (*n* = 3). The SD of both red and green distributions is 22%. (*I–L*) Parasagittal sections of the SC from WT (*I* and *K*) or Math5$^{-/-}$ (*J* and *L*) mice in which RGCs were labeled by a focal injection of DiI in the temporal (*I* and *J*) and nasal (*K* and *L*) retina results in single termination zones in the anterior and posterior SC, respectively, of WT mice, but broader termination zones in Math5$^{-/-}$ mice (*n* = 3). (Scale bar, 100 μm.)
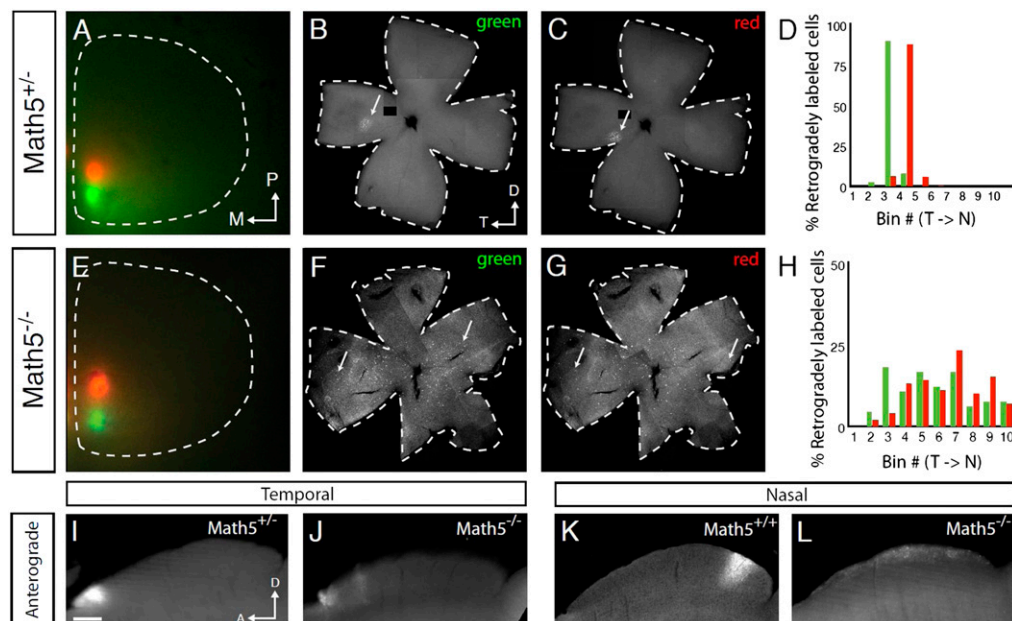
We tested this possibility in a number of ways. We find that RGCs in Math5$^{-/-}$ mice make correct pathfinding decisions and project to the same visual areas as their WT counterparts, suggesting that axon pathfinding proteins and target selection cues are expressed normally and functionally in Math5$^{-/-}$ RGCs and their targets (*SI Appendix*, Fig. S10). In addition, we find that Math5$^{-/-}$ mice display asymmetric expression of EphAs/ephrin-As and EphB/ephrin-Bs in the retina as well as relatively normal EphA, ephrin-A, Cadherin-8, and Odz3 expression in the SC. This suggests that overall patterning of the retina and SC is not affected by the Math5 mutation. However, because RNA levels revealed by in situ hybridization relate indirectly to the protein levels and because we cannot distinguish between RGCs and displaced amacrine cells in the ganglion cell layer of the retina, we cannot accurately compare the slopes of the gradients within the RGCs of the various markers.

We also determined that individual RGCs in Math5$^{-/-}$ mutants have physiological properties similar to those of WT RGCs during times in development when RGCs discharge highly correlated bursts of activity that propagate across the retina as waves. These patterns of activity have been proposed to drive refinement through activity-dependent mechanisms and are incorporated into our modeling (36–38). Defects in refinement occur when the structure of retinal waves is disrupted in a mouse lacking the β2 subunit of the nACh receptor (β2$^{-/-}$ mouse) (39–41). Using a large-scale, multielectrode array to isolate single-unit responses from RGCs, we find that Math5$^{-/-}$ RGCs are capable of firing bursts of action potentials in patterns similar to those of WT RGCs. When we calculated the correlation index (CI) (*SI Appendix, SI Methods*) in the spiking between RGC pairs as function of the distance between them, we find that the CI for pairs of Math5$^{-/-}$ RGCs is large (more that fivefold above chance) for neurons separated by less that 400 μm, which decreases to that of chance by 1 mm. Interestingly, at distances between 450–800 μm, the CI is lower than in WT retina (*SI Appendix*, Fig. S6). Because these recordings are done in vitro and it has been shown that the spiking properties of RGCs can vary with media composition or temperature (42, 43) these differences may not be reflective of RGC firing in vivo. To test

whether the compression of the map in Math5 mutants is a result of altered wave activity, we created a Math5/β2 double mutant and traced its RGC projections. We find that the compression of the map in the SC is not changed in Math5/β2 double mutants, indicating that map compression is not affected by the exact pattern of spontaneous activity during development (*SI Appendix*, Fig. S11). However, a change in activity patterns of Math5 RGCs could explain the lack of refinement of their axons observed in our anterograde tracing studies in Fig. 4.

Discussion

Here we show that axon–axon competition is a driving force for topographic mapping of the mouse retinocollicular projection, through both theoretical and experimental approaches. We assayed the effects of reduced competition by comparing the RGC projections in WT and Math5 mutant mice, which have severely reduced numbers of RGCs. Thus, we studied the role of competition in mammals without using lesion experiments. We show that our experimental results are strikingly similar to simulations of retinocollicular map formation if competition is invoked as the counterbalancing force along each axis. Despite the fact that all alternative models include an identical form of competition, the distortions of topography in these models are either minor or are not consistent with experimental data. We conclude that the chemoaffinity mechanism involved in the development of topographic maps alone cannot specify correct axon positions and relies on competition as a necessary supplement.

We propose that along the T–N mapping axis, a single ephrin-A repellent gradient is counterbalanced by competition between axons to yield an ordered topographic map, whereas along the D–V axis, a medially derived attractant gradient is counterbalanced by competition to yield an ordered topographic projection. This model is in agreement with our result in Math5$^{-/-}$ mouse that shows an accumulation of axons in the anteromedial SC in the absence of competition.

Although previous mapping studies in ephrin/Eph mutant mice are consistent with the competition model proposed here, they are also consistent with the servomechanism and dual gradient models (44). Thus, map expansions and contractions

NEUROSCIENCE

observed after retinal and tectal/collicular ablations (45–49), when competition between axons is modified, are consistent with the dual gradient, servomechanism, and competition models, because each includes competition as a mechanism to ensure uniform target coverage (4, 21). Perhaps for this reason, recent reviews of mapping in the literature present the prevailing model for the topographic map formation as a dual gradient model along the A–P axis and a form of servomechanism along the M–L axis (50, 51).

Previous attempts to reduce competition in mammals using tissue ablation of the retina or SC have not always led to consistent rearrangements seen in lower vertebrates (20, 52). This may be due to the technical challenges in creating reproducible lesions and the possibility that neural damage could affect axon mapping. In Brn3b mutant mice, whose retinas contain about 20% of the WT number of RGCs, the axons of remaining cells spread out and fill the entire target (53), which is similar to the effects of lesions in lower vertebrates. Interestingly, our model predicts that a loss of 80% of RGCs will have relatively minor defects in topography (*SI Appendix*, Fig. S7), in agreement with the observations in Brn3b mutant mice (53). This means that axonal competition is a potent mapping mechanism capable of redistributing cells over their target even when a substantial fraction of cells is removed. Here we further reduce competition by studying the Math5$^{-/-}$ mice that retain only 5–10% of the WT number of RGCs. We observe severe distortions in the retinocollicular projection that are consistent with the axonal competition reaching its limit and becoming incapable of filling the target. These distortions suggest that axonal competition is a nonredundant mapping mechanism that, along with a single gradient of chemical labels, is necessary to determine the axonal termination zones. Our results also suggest that axon–axon competition is a means by which RGC axons read relative but not absolute levels of ephrin-As in the SC in vivo (14).

A mapping mechanism based on competition and a single gradient of molecular labels per axis advocated here was recently challenged in zebrafish (24), in which transplantation methods were used to create fish with eyes containing a single RGC. When single RGCs were traced into the tectum, the distal (posterior) tips of arbors were found at retinotopically appropriate positions, suggesting that axons can project topographically without other axons present. At the same time, the proximal (anterior) branches of the arbors extended into topographically inappropriate anterior tectum. When we simulated the formation of the retinotectal projection in the conditions of a single axon present (as in ref. 24), we find that the competition model can explain the results observed in the zebrafish with a solitary axon, including both the topographically placed distal branches and anteriorly displaced proximal branches (*SI Appendix*, Fig. S8). The topographic placement of the distal (posterior) branches of a singular axon is expected, because an axon that carries low levels of EphA (nasal) can propagate deeper into the target than axon with high level of EphA (temporal) (*SI Appendix*, Fig. S8). Therefore, we suggest that the observations in zebrafish with a singular RGC are consistent with the competition mapping mechanism presented here.

Whereas our results are most consistent with competition models for topography, they do not fit perfectly, especially along the A–P axis. In the simulations, axonal terminals occupy an area that becomes narrower posteriorly (Fig. 2*B*); however, the region occupied by axons widens somewhat in the posterior direction (Fig. 3*C*). This behavior is consistent with a more complex distribution of attractants in the SC that becomes wider in the posterior direction. Such behavior was not included in the model, in which the distribution of chemoattractant (ephrin-B) was assumed to be dependent only on the medial–lateral coordinate, which may be an oversimplification of the EphB/ephrin-B expression pattern (54). Another mismatch between model predictions and experimental

results occurs near the anterior edge of SC, where axons deviate slightly from the area boundary. These differences could be explained by a somewhat smooth distribution of markers that define the boundary, which was assumed to be infinitely sharp in the model. Another intriguing explanation of this discrepancy is the possibility that a second factor as predicted in the dual gradient or servomechanism models has minor influences on axons or on a distinct subset of RGCs. For example, it has been proposed that p75 is a coreceptor for retinal ephrin-A reverse signaling, and mutants lacking p75 in the retina make minor topographic errors with nasal axons shifting slightly anteriorly (30, 31). We suggest that our data are consistent with a model that reverse signaling is not strong enough to provide a counterbalancing force for the repulsive effects of the ephrin-A gradient, and that competition between axons is required for this purpose. The role of reverse signaling could be to adjust the magnification factor of retinocollicular maps by shifting axons slightly posteriorly. The competition model proposed here could include a second factor as in the dual gradient model, provided it is sufficiently weak, without substantially changing its behavior.

Our experiments indicate that the D–V retinal axis is mapped by a single gradient plus competition. One model for mapping this axis is based on a bifunctionality of ephrin-Bs to act as both attractants and repellents, represented in this study by the servomechanism model (Fig. 2 *E–G*). This model predicts that when competition is reduced, as in Math5$^{-/-}$ mice, mapping along the D–V axis remains intact. In contrast, we observe a substantial medial shift of projections in Math5$^{-/-}$ mice. Because there is a substantial enrichment of RGCs in the medial SC, we predict that there is either a lateral-to-medial repellent activity or a medial-to-lateral attractant activity in the SC. This enrichment is consistent with ephrin-Bs providing an attractive force that peaks in medial SC or with other molecules that could act as a medially derived attractant. Our findings are inconsistent with models proposing that ephrin-Bs act bifunctionally as repellents and attractants toward EphB bearing axons or that the attraction of ephrin-Bs is counterbalanced by a gradient of Wnt repellent activity (13, 55).

Axon–axon competition ensures that the entirety of a target space gets filled and is also important for synapse refinement at the neuromuscular junction (56). Here we show that axon competition can counterbalance a single molecular gradient and thereby act as a necessary factor in topographic mapping. Given that gradient-based topographic mapping is likely common to all mammalian sensory pathways and structures, the competition-based mechanism we propose here may be a basic mechanistic feature of CNS wiring in mammals.

Materials and Methods

Computational Procedures. To model the development of the retinocollicular projection, we used a method based on minimization of effective affinity potential, which is a function of the synaptic connectivity matrix between the retina and SC. Specific details of the modeling are provided in the *SI Appendix*.

Experimental Procedures. *Mice.* Math5 and β2 mutant mice were genotyped using PCR as described (35, 57).

Axon tracing. Whole eye labeling of adult and early postnatal mice was done as described (58). Images were captured with an AxioCam Hrm digital camera through a 5× objective on an Axioskop 2 Plus microscope (Zeiss), photographed as a whole mount with the cortex removed, or from 100-μm-thick vibratome sections. Retrograde and anterograde tracing was as follows: 0.2–1 μL of CTB-555 or CTB-488 was injected into the SC of P8–P10 mice. Two days later, the contralateral retina was visualized as a flat mount, RGC layer side up and photographed using a digital camera through a 2.5× or 5× objective on an Axioskop 2 Plus microscope (Zeiss). Anterograde tracing was done as described (57).

Quantification of fluorescence distribution in the SC. Images of the SC, fluorescently labeled by whole eye fill, were processed using ImageJ (http://rsb.info.nih.gov/ij/). Background was reduced using a rolling ball filter of 300 pixels. To determine the fluorescence distribution across the A–P and L–M

axes, a rectangular region equal to (*i*) the height of the anatomical A–P axis by one-third the total anatomical width of the SC, positioned with the outside edge aligned with the medial boundary of the SC or (*ii*) the total anatomical width and one-third the total anatomical length of the A–P axis centered over the position of maximum intensity in M5$^{-/-}$ mice, roughly one-third the total A–P length posterior of the anterior edge, was selected. Intensity values were calculated along each region using the "Plot Profile" tool. Fluorescence intensity values were percentile ranked along the A–P or L–M axes for each mouse, such that the anterior and medial edges of the SC equal 0% the total intensity and the posterior and lateral edges are 100%. Statistical significance was calculated using the Kolmogorov–Smirnoff test. Because of the posterior widening of the projection (Fig. 3*C*), some of the labeling shifts laterally from the rectangular region and is not counted

toward the rank in Fig. 3*D*. We have estimated that the associated errors in percentile rank are less than 3%.

1. Lewin B (1994) On neuronal specificity and the molecular basis of perception. *Cell* 79: 935–943.
2. Rakic P (1981) Development of visual centers in the primate brain depends on binocular competition before birth. *Science* 214:928–931.
3. Cang J, Wang L, Stryker MP, Feldheim DA (2008) Roles of ephrin-as and structured activity in the development of functional maps in the superior colliculus. *J Neurosci* 28 (43):11015–11023.
4. Gierer A (1983) Model for the retino-tectal projection. *Proc R Soc Lond B Biol Sci* 218: 77–93.
5. Prestige MC, Willshaw DJ (1975) On a role for competition in the formation of patterned neural connexions. *Proc R Soc Lond B Biol Sci* 190:77–98.
6. Hornberger MR, et al. (1999) Modulation of EphA receptor function by coexpressed ephrinA ligands on retinal ganglion cell axons. *Neuron* 22:731–742.
7. Knöll B, Zarbalis K, Wurst W, Drescher U (2001) A role for the EphA family in the topographic targeting of vomeronasal axons. *Development* 128:895–906.
8. Yates PA, Holub AD, McLaughlin T, Sejnowski TJ, O'Leary DD (2004) Computational modeling of retinotopic map development to define contributions of EphA-ephrinA gradients, axon-axon interactions, and patterned activity. *J Neurobiol* 59:95–113.
9. Fraser SE, Hunt RK (1980) Retinotectal specificity: Models and experiments in search of a mapping function. *Annu Rev Neurosci* 3:319–352.
10. Hansen MJ, Dallal GE, Flanagan JG (2004) Retinal axon response to ephrin-as shows a graded, concentration-dependent transition from growth promotion to inhibition. *Neuron* 42:717–730.
11. Honda H (1998) Topographic mapping in the retinotectal projection by means of complementary ligand and receptor gradients: A computer simulation study. *J Theor Biol* 192:235–246.
12. Honda H (2003) Competition between retinal ganglion axons for targets under the servomechanism model explains abnormal retinocollicular projection of Eph receptor-overexpressing or ephrin-lacking mice. *J Neurosci* 23(32):10368–10377.
13. McLaughlin T, Hindges R, Yates PA, O'Leary DD (2003) Bifunctional action of ephrin-B1 as a repellent and attractant to control bidirectional branch extension in dorsal-ventral retinotopic mapping. *Development* 130:2407–2418.
14. Brown A, et al. (2000) Topographic mapping from the retina to the midbrain is controlled by relative but not absolute levels of EphA receptor signaling. *Cell* 102: 77–88.
15. Feldheim DA, et al. (1998) Topographic guidance labels in a sensory projection to the forebrain. *Neuron* 21:1303–1313.
16. Koulakov AA, Tsigankov DN (2004) A stochastic model for retinocollicular map development. *BMC Neurosci* 5:30.
17. Tsigankov DN, Koulakov AA (2006) A unifying model for activity-dependent and activity-independent mechanisms predicts complete structure of topographic maps in ephrin-A deficient mice. *J Comput Neurosci* 21:101–114.
18. Tsigankov D, Koulakov A (2009) Optimal axonal and dendritic branching strategies during the development of neural circuitry. *Front Neural Circuits* 3:18.
19. Tsigankov D, Koulakov AA (2010) Sperry versus Hebb: Topographic mapping in Isl2/EphA3 mutant mice. *BMC Neurosci* 11:155.
20. Finlay BL, Schneps SE, Schneider GE (1979) Orderly compression of the retinotectal projection following partial tectal ablation in the newborn hamster. *Nature* 280: 153–155.
21. Fraser SE, Perkel DH (1990) Competitive and positional cues in the patterning of nerve connections. *J Neurobiol* 21:51–72.
22. Simon DK, O'Leary DDM (1992) Development of topographic order in the mammalian retinocollicular projection. *J Neurosci* 12:1212–1232.
23. Feldheim DA, et al. (2004) Loss-of-function analysis of EphA receptors in retinotectal mapping. *J Neurosci* 24(10):2542–2550.
24. Gosse NJ, Nevin LM, Baier H (2008) Retinotopic order in the absence of axon competition. *Nature* 452:892–895.
25. Brown NL, et al. (1998) Math5 encodes a murine basic helix-loop-helix transcription factor expressed during early stages of retinal neurogenesis. *Development* 125: 4821–4833.
26. Saul SM, et al. (2008) Math5 expression and function in the central auditory system. *Mol Cell Neurosci* 37:153–169.
27. Lin B, Wang SW, Masland RH (2004) Retinal ganglion cell type, size, and spacing can be specified independent of homotypic dendritic contacts. *Neuron* 43:475–485.
28. Monschau B, et al. (1997) Shared and distinct functions of RAGS and ELF-1 in guiding retinal axons. *EMBO J* 16:1258–1267.
29. Nakamoto M, et al. (1996) Topographically specific effects of ELF-1 on retinal axon guidance in vitro and retinal axon mapping in vivo. *Cell* 86:755–766.
30. Lim YS, et al. (2008) p75(NTR) mediates ephrin-A reverse signaling required for axon repulsion and mapping. *Neuron* 59:746–758.
31. Marler KJ, et al. (2008) A TrkB/EphrinA interaction controls retinal axon branching and synaptogenesis. *J Neurosci* 28(48):12700–12712.
32. Rashid T, et al. (2005) Opposing gradients of ephrin-As and EphA7 in the superior colliculus are essential for topographic mapping in the mammalian visual system. *Neuron* 47:57–69.
33. Hindges R, McLaughlin T, Genoud N, Henkemeyer M, O'Leary DD (2002) EphB forward signaling controls directional branch extension and arborization required for dorsal-ventral retinotopic mapping. *Neuron* 35:475–487.
34. Braisted JE, et al. (1997) Graded and lamina-specific distributions of ligands of EphB receptor tyrosine kinases in the developing retinotectal system. *Dev Biol* 191:14–28.
35. Brown NL, Patel S, Brzezinski J, Glaser T (2001) Math5 is required for retinal ganglion cell and optic nerve formation. *Development* 128:2497–2508.
36. Butts DA (2002) Retinal waves: Implications for synaptic learning rules during development. *Neuroscientist* 8:243–253.
37. Meister M, Wong RO, Baylor DA, Shatz CJ (1991) Synchronous bursts of action potentials in ganglion cells of the developing mammalian retina. *Science* 252:939–943.
38. Wong ROL, Meister M, Shatz CJ (1993) Transient period of correlated bursting activity during development of the mammalian retina. *Neuron* 11:923–938.
39. Cang J, et al. (2005) Ephrin-as guide the formation of functional maps in the visual cortex. *Neuron* 48:577–589.
40. Chandrasekaran AR, Plas DT, Gonzalez E, Crair MC (2005) Evidence for an instructive role of retinal activity in retinotopic map refinement in the superior colliculus of the mouse. *J Neurosci* 25(29):6929–6938.
41. McLaughlin T, Torborg CL, Feller MB, O'Leary DD (2003) Retinotopic map refinement requires spontaneous retinal waves during a brief critical period of development. *Neuron* 40:1147–1160.
42. Stafford BK, Sher A, Litke AM, Feldheim DA (2009) Spatial-temporal patterns of retinal waves underlying activity-dependent refinement of retinofugal projections. *Neuron* 64:200–212.
43. Sun C, Warland DK, Ballesteros JM, van der List D, Chalupa LM (2008) Retinal waves in mice lacking the beta2 subunit of the nicotinic acetylcholine receptor. *Proc Natl Acad Sci USA* 105:13638–13643.
44. Clandinin TR, Feldheim DA (2009) Making a visual map: Mechanisms and molecules. *Curr Opin Neurobiol* 19:174–180.
45. Attardi DG, Sperry RW (1963) Preferential selection of central pathways by regenerating optic fibers. *Exp Neurol* 7:46–64.
46. Sharma SC, Romeskie M (1977) Immediate 'compression' of the goldfish retinal projection to a tectum devoid of degenerating debris. *Brain Res* 133:367–370.
47. Cook JE (1979) Interactions between optic fibres controlling the locations of their terminals in the goldfish optic tectum. *J Embryol Exp Morphol* 52:89–103.
48. Schimidt JT, Cicerone CM, Easter SS (1978) Expansion of the half retinal projection to the tectum in goldfish: An electrophysiological and anatomical study. *J Comp Neurol* 177:257–277.
49. Yoon M (1971) Reorganization of retinotectal projection following surgical operations on the optic tectum in goldfish. *Exp Neurol* 33:395–411.
50. Flanagan JG (2006) Neural map specification by gradients. *Curr Opin Neurobiol* 16: 59–66.
51. O'Leary DD, McLaughlin T (2005) Mechanisms of retinotopic map development: Ephs, ephrins, and spontaneous correlated retinal activity. *Prog Brain Res* 147:43–65.
52. Simon DK, Roskies AL, O'Leary DDM (1994) Plasticity in the development of topographic order in the mammalian retinocollicular projection. *Dev Biol* 162:384–393.
53. Badea TC, Cahill H, Ecker J, Hattar S, Nathans J (2009) Distinct roles of transcription factors brn3a and brn3b in controlling the development, morphology, and function of retinal ganglion cells. *Neuron* 61:852–864.
54. Scalia F, Feldheim DA (2005) Eph/ephrin A- and B-family expression patterns in the leopard frog (Rana utricularia). *Brain Res Dev Brain Res* 158:102–106.
55. Schmitt AM, et al. (2006) Wnt-Ryk signalling mediates medial-lateral retinotectal topographic mapping. *Nature* 439:31–37.
56. Barber MJ, Lichtman JW (1999) Activity-driven synapse elimination leads paradoxically to domination by inactive neurons. *J Neurosci* 19(22):9975–9985.
57. Pfeiffenberger C, Yamada J, Feldheim DA (2006) Ephrin-As and patterned retinal activity act together in the development of topographic maps in the primary visual system. *J Neurosci* 26(50):12873–12884.
58. Pfeiffenberger C, et al. (2005) Ephrin-As and neural activity are required for eye-specific patterning during retinogeniculate mapping. *Nat Neurosci* 8:1022–1027.

NEUROSCIENCE